X-ray beam-position monitoring in the sub-micrometre and sub-second regime

Oliver Bunk,[a]* Franz Pfeiffer,[a] Marco Stampanoni,[a] Bruce D. Patterson,[a] Clemens Schulze-Briese[a] and Christian David[b]

[a]Paul Scherrer Institut, Swiss Light Source, 5232 Villigen PSI, Switzerland, and [b]Paul Scherrer Institut, Laboratory for Micro- and Nanotechnology, 5232 Villigen PSI, Switzerland.
E-mail: oliver.bunk@psi.ch

It is demonstrated that X-ray beam positions can be extracted from two-dimensional profiles with sub-pixel resolution. Beam-position measurements utilizing a self-designed low-cost two-dimensional detector have been performed at two synchrotron radiation beamlines of the Swiss Light Source. The effective detector pixel size was 4.8 μm and the resolution achieved for the beam position was about 5 nm. At a data rate of 25 frames per second, periodic variations of the beam position could be detected with a frequency resolution below 0.1 Hz. This allowed, for example, the influence of a turbo-pump in the X-ray optics hutch on the beam position to be quantified, and even minute variations related to the electron beam in the storage ring could be detected.

Keywords: X-ray beam position; X-ray camera; sub-pixel resolution; diagnostic tool.

1. Introduction

At third-generation synchrotron radiation sources, X-ray beam sizes in the micrometre regime are routinely achieved. Pre-requisite for utilizing these microbeams is an X-ray beam-position stability in the sub-micrometre regime. State-of-the-art electron and photon beam-position monitors (BPMs) are necessary to achieve such an outstanding stability (Shu *et al.*, 1998; Holldack *et al.*, 2001; Kudo *et al.*, 2001). The Swiss Light Source (SLS) is operated in 'top-up mode' with injections at intervals of typically 1–2 min, to keep the ring current (presently 350 mA) constant to within 1 mA, *i.e.* to within 0.3%. Within one top-up run of several days and not considering the short injection periods, the long-term positional deviation from the 'golden orbit' is below 1 μm (root-mean-square, RMS). This demonstrates that a good foundation for excellent photon beam stability is laid by state-of-the-art machines (Schilcher *et al.*, 2004; Böge, 2004). In this article, we will deal with photon rather than electron beam stability. One class of photon BPM is formed by the non-intercepting devices (Billing, 1988) that either interfere only with outer parts of the photon beam or at least transmit the major part of the incident intensity. Among the various devices are wire (Heald, 1986; Karlin *et al.*, 1992), blade (Mortazavi *et al.*, 1986; Holldack *et al.*, 2001; Xie *et al.*, 2001), split-plate ion chamber (Tischler & Hartman, 1980; Schildkamp & Pradervand, 1995), chemically vapour-deposited diamond (Sakae *et al.*, 1997; Bergonzo *et al.*, 1999; Schulze-Briese *et al.*, 2001), metal-foil and diode (Silfhout, 1999; Alkire *et al.*, 2000) and Be-diffraction (Fajardo & Ferrer, 1995) BPMs. Spatial resolution in the micrometre

regime at a data rate of several Hertz is routinely achieved and used in feedback-loop systems to stabilize the beam position. In general, there is a trade-off between spatial resolution and data rate. Detection with sub-second resolution becomes exceedingly important with the advance of techniques like X-ray photon correlation spectroscopy (Lurio *et al.*, 2000).

In this article we demonstrate a simple low-cost diagnostic tool that allows two-dimensional beam-position detection with, in the case of our first test system, sub-micrometre resolution at a repeat rate of 25 Hz. The system fills a gap in the set of tools necessary in the commissioning phase of new beamline components. We demonstrate this by showing that fingerprints of a turbo-pump in the optics hutch of a synchrotron beamline, and even of the booster for the electron beam (Schilcher *et al.*, 2004; Böge, 2004), can be detected. It is not our intention to investigate long-term X-ray beam stability with this method. For this application the existing slow BPMs are well suited. The focus in this article is on comparisons, for example with and without a certain vibration source, and on characteristic fingerprints in the power spectrum.

2. Experimental

The basic idea is to use a fast two-dimensional X-ray camera (Koch & Riekel, 1996) as a detector and combine it with a data analysis that uses the fact that the, typically Gaussian, shape of the X-ray beam is known, to achieve a spatial resolution far below the size of a detector pixel.

research papers

2.1. Detector system

The first test system consisted of a 170 µm-thick YAG scintillator to convert the X-rays into visible light, a lens system that transmits the light onto the CCD chip of the camera, and a frame-grabber to re-digitize the data for display and analysis on a PC system. We used an eight-bit camera with 1/3" chip and 25 Hz frame rate (EHDkamPro03, EHD, Germany), and a standard frame-grabber (DFG/1394-1, The Imaging Source, USA/Germany). The reason for constructing our own detector system instead of using a commercial assembly is twofold: (i) the design allows us to control the magnification and thereby the effective pixel size and the field of view *via* the lens system; (ii) it is considerably cheaper than assembled systems 'in a box'. The system is shown in Fig. 1. The combination of lenses and 1/3" CCD chip results in a field of view of 3.8 mm × 2.8 mm with 768 × 576 square pixels of 4.8 µm effective size, about three-quarters of the CCD pixel size of 6.3 µm. A similar device specified up to 10 Hz is available from SESO, France (SESO, http://www.seso.com/pub/X%20Ray%20Beam%20Monitor.pdf).

2.2. Measurements

To test the set-up, we recorded 1 min 'movies' of the monochromatic beam at two SLS beamlines, namely the Protein Crystallography I (PXI, X06SA) and the Materials Science (MS, X04SA) beamlines. To ease data processing, the monochrome 'movies' were saved in RGB24 format, resulting in 2 Gbyte of data per 1 min recording time. Lossless compression *via* a video codec (Huffyuv by Ben Rudiak-Gould) allowed for smaller file sizes, as long as the data processing was restricted to systems supported by the codec. To test the stability of the algorithms and for the sake of simplicity, the recorded data were neither dark-image nor flat-field corrected although these corrections would have had a positive effect on the resolution.

At the PXI beamline, an in-vacuum undulator generates the spectrum and the photon energy is set by a liquid-nitrogen-cooled Si(111) double-crystal monochromator. The monochromator was set to 14.4 keV, corresponding to a wavelength of 0.86 Å, and both the sagittally focusing second monochromator crystal and the vertically focusing mirror bender were set in a way that the beam was slightly focused. The
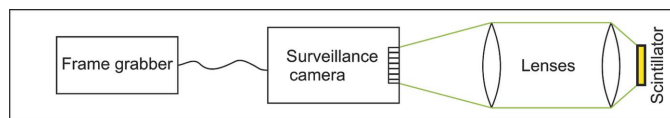
beamline is designed for a modest demagnification of 2.5:1 at the position of the high-resolution diffractometer, 28 m from the source point. Only the upstream slit system was used to define the beam to avoid falsification of the results by cutting parts of the beam with downstream slit systems. The camera was placed on the table for the micro-diffractometer, approximately 22.5 m from the source point.

The question specifically addressed at this beamline was whether there are instabilities of the beam position that could degrade the recently measured transverse coherence (Pfeiffer *et al.*, 2005), especially on short time scales within typical detector exposure and BPM delay times.

At the MS beamline, a mini-gap wiggler and a Si(111) double-crystal monochromator of the TORII type with water cooling are installed. Mirrors in front of and after the monochromator can be used to collimate and focus the beam. Details can be found elsewhere (Patterson *et al.*, 2005). The monochromator was set to 12.4 keV, corresponding to 1.0 Å, and the beam was focused to a size at the detector position that allowed using the full field-of-view of the X-ray camera system. The X-ray camera was placed on the optical table for the tomography set-up. At this position, 32 m from the source, an approximately 1:1 image of the source is seen. At the MS beamline, we specifically searched for a source of aperiodic beam-position instabilities.

As examples for typical data, a beam profile and the horizontal position as a function of time resulting from the analysis are shown in Fig. 2. The RMS value after subtraction of the
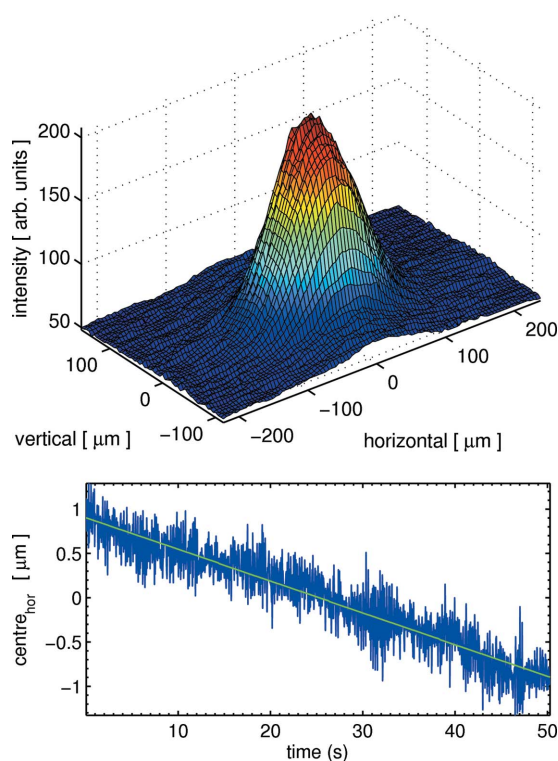
Figure 2
Top: three-dimensional surface plot of the beam profile as recorded at the PXI beamline X06SA. Bottom: short-term drift of the horizontal beam position at the PXI beamline (source unknown). The straight line marks a line-fit with a slope of 36 nm s^{-1}.

Figure 1
The low-cost detector set-up consisting of (from right to left) scintillator, lens system, CCD camera and frame-grabber.

linear trend is 0.2 µm. This value is not solely determined by noise; it includes a low-amplitude signal as discussed below.

2.3. Data analysis

The algorithm for the data analysis should be sufficiently simple to allow for a straightforward implementation in the various beamline control systems. It should be fast enough to give results either on-line or at least with only short delays. Finally it should be robust against artifacts and give reproducible results.

The common feature of the algorithms tested is that they use the full two-dimensional information to determine the beam position with sub-pixel resolution. Four algorithms have been compared: (i) 'centre-of-mass', a simple centre-of-mass or centroid calculation; (ii) 'statistical', an algorithm that determines the beam position as the centre between the interpolated full-width-at-half-maximum (FWHM) positions; (iii) '1D Gauss', two one-dimensional Gaussian fits horizontal and vertical; (iv) '2D Gauss', a two-dimensional Gaussian fit.

Methods (i) to (iii) operate on sums of rows or columns, whereas (iv) is a true two-dimensional method. A linear background has been taken into account in cases (ii) and (iii), but this turned out to be unnecessary, a constant background would have been sufficient. The algorithms (i) and (ii) are sufficiently fast for on-line data analysis, (iii) is still rather fast, whereas (iv) is only suitable for off-line data analysis. Only a qualitative comparison of the calculation speed is given, since the absolute numbers depend on factors like the detector resolution and the programming or scripting language used for the analysis.

3. Results and discussion

Part of the study was intended to find the most suitable algorithm for determining the two-dimensional beam position from the recorded data, in terms of both precision and speed.

3.1. Algorithms

Each algorithm was used to determine the horizontal and vertical beam position for each of the approximately 1500 frames recorded within the measurement interval of 60 s. All algorithms except the centre-of-mass method give additional information about the horizontal and vertical FWHM, peak intensity and background level. For each of the determined quantities, the power spectrum, i.e. the absolute value of the discrete Fourier transform, was calculated.

As an example, the power spectrum of the horizontal beam position for the PXI beamline is shown in Fig. 3, as determined using the four algorithms compared in this study.

It is rather obvious that the centre-of-mass algorithm failed completely. The feature around 8.7 Hz was detected by all methods except the centre-of-mass analysis. The method works better if it is only applied in a region of interest that is rather narrowly defined around the beam position. But to improve the algorithm in this way, one needs a rough estimate of the beam position prior to a more precise determination by the centre-of-mass algorithm. The advantages of the method, its simplicity and independence of the peak shape, are lost in this way, and the data are still not sufficient for a detailed frequency analysis. We conclude that the centre-of-mass algorithm is only useful if intensity features are analyzed that are absolutely irregular and non-Gaussian, i.e. features that cannot be analyzed with the other algorithms.

The one-dimensional Gauss analysis leads to a less noisy spectrum than the statistical method. But the power spectrum is still too noisy to determine unambiguously whether the sharp spike at 3.13 Hz is real or just an artifact. The feature at 8.7 Hz is detected by both methods.

Only the two-dimensional Gauss fit results in a power spectrum with sufficiently low noise to reveal that the spike at 3.13 Hz is real. The main component around 8.7 Hz and also the feature around 12.5 Hz are not better resolved than with the one-dimensional Gauss and the statistical method.

We conclude that for fast on-line analysis the statistical method is the best choice, since the slower one-dimensional Gauss fit does not bring an improvement worth the additional calculation time. For data of very low noise level and the detection of tiny well defined features, there is no alternative to the slow two-dimensional Gaussian fit.

The techniques have an astonishing precision: the beam-position data shown in Fig. 2 are not as noisy as they look on first sight. The position oscillates periodically, thereby causing the feature in the power spectrum around 8.7 Hz (Fig. 3). The RMS value of the horizontal beam position after linear trend subtraction, containing both signal and noise, is 0.2 µm. Obviously the spatial resolution is therefore significantly better than 0.2 µm.

The frequency of the 3.13 Hz oscillation is far better defined than the feature at 8.7 Hz. The explanation for this significant difference is that 3.13 Hz is the frequency of the booster for the electron beam. Hence a well defined feature of the electron beam is detected via the photon beam. The corresponding spike in the power spectrum is only a single point of close to 20 nm amplitude, i.e. the integrated power is in this case equal
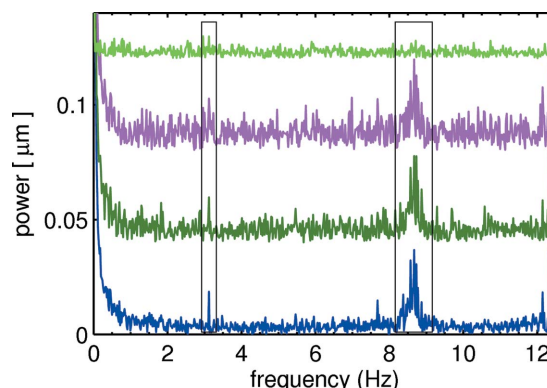
Figure 3
Comparison of the data-analysis algorithms. Shown is the power spectrum of the horizontal beam position at the PXI beamline calculated using the (from bottom to top) 2D Gauss, 1D Gauss, statistical and centre-of-mass algorithms. The graphs are offset by 0.04 µm for clarity. Two features discussed in the text are marked with a box.

to the peak value. That means that an oscillation with an amplitude of 20 nm, less than 1/200 of the effective detector pixel size, is detected with this simple method. The detection limit is given by the background level; it is below 5 nm in that frequency region, *i.e.* 1/1000 of the effective detector pixel size.

3.2. Results for the PXI and MS beamline

The power spectrum of the horizontal beam position both at the PXI (Fig. 3) and the MS beamline (Fig. 4) exhibit the spike at 3.13 Hz, corroborating that this is a feature of the electron beam seen at all beamlines rather than an instability caused by the individual quite different beamline optics. The source of the 8.7 Hz perturbation at the PXI beamline has to be investigated further, but the stronger 4.5 Hz perturbation at the MS beamline has been identified unambiguously. It is caused by a turbo-pump in the optics hutch of the beamline and vanished after the pump was switched off (see Fig. 4). Special precautions had been undertaken to reduce any influence of that pump by mechanically decoupling it from the main system. Without the fast detection method and the detailed frequency analysis presented here, the beam-position oscillations caused by this pump could so far not be detected. Nevertheless, the identification of this source of vibrations was very important for the beamline, since the aperiodic stronger beam-position movements seen before also vanished after the pump had been switched off. That means, even if one is not concerned about spatial resolution in the micrometre regime, this diagnostic tool can provide valuable information.

Additionally it has been found that reducing the cooling water flow to the MS beamline monochromator causes aperiodic instabilities (not shown). In this way it is straightforward to determine the optimum flow for sufficient cooling without inducing additional vibrations.
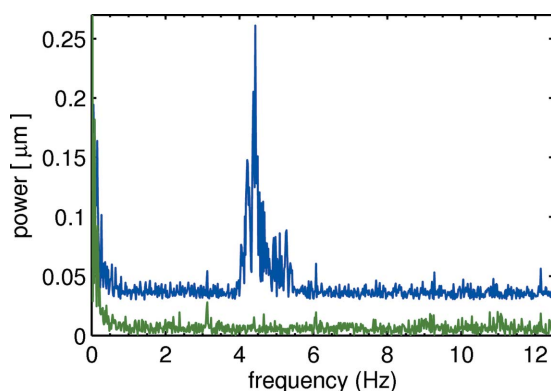
3.3. Strengths and limitations

The strength of the present method is the high spatial resolution achieved with standard equipment. The lens system can be used to reduce the effective pixel size. The data analysis increases the resolution, defined as the noise level in the

power spectrum, further by roughly a factor of 1000. In this sub-micrometre regime many factors may influence the resolution. Owing to the thickness of the scintillator and cross-talk between CCD pixels, the true pixel size will be larger than the effective size calculated as the field of view divided by the pixel size. Noise of the original data will influence the peak position detection. That the precision of the peak detection depends on the algorithm is clearly visible in Fig. 3. For long-term measurements with sub-micrometre resolution, the mounting of the detection system and temperature stability clearly become important issues. We have not undertaken efforts to quantify these influences on the spatial resolution since they are less important in the case of comparative short-term and frequency fingerprint studies that are the aim of our investigation. Additionally, the above-given values for the apparent spatial resolution as judged from the quality of the data are absolutely sufficient for our purposes.

Another important advantage of the present method is the data rate. Our test system recorded data with 25 frames per second, and in the meantime cameras are available that allow several 100 Hz. The unambiguous detection of frequencies is, according to Shannon's sampling theorem, limited to the Nyquist frequency that is half the sampling frequency. But perturbations at higher frequency are not undetected, just their frequency is not correctly assigned, which may hamper the identification of the vibration source. Only frequencies that are exactly multiples of the sampling frequency are undetected, since they cannot be distinguished from the constant base-line. The only obvious disadvantage of the method is that it intercepts the whole beam. It can, for example, be used as a valuable diagnostic tool in the commissioning phase for new equipment or to characterize the stability from time to time.

For periodic signals, the frequency resolution is determined by the recording time. The 1 min recording time chosen here is sufficient for a frequency resolution well below 0.1 Hz, *i.e.* significantly better than that necessary to identify sources of vibration at the beamline.

4. Summary

An X-ray camera system for measuring two-dimensional monochromatic beam profiles at 25 Hz is presented. A simple and fast 'statistical' data-analysis algorithm can be used to determine the two-dimensional beam position and full width at half-maximum with sub-pixel resolution. A slow two-dimensional Gaussian fit reduces significantly the noise of the data, though this is only necessary for the detection of minor components in the power spectrum. The noise level of the power spectra is about 5 nm in the present case. The identification of a source of vibrations and even of the booster frequency of the Swiss Light Source is demonstrated. The system is ideally suited to detect and minimize vibrations of beamline components.

Figure 4
Power spectrum of the horizontal beam position at the MS beamline with a turbo-pump in the optics hutch switched on (top) and off (bottom). The graphs are offset by 0.03 µm for clarity.

5. Outlook

We are currently commissioning a camera with a frame rate faster than 100 Hz to allow the unambiguous detection of 50 Hz frequencies, a typical frequency caused by electronic equipment. First test measurements showed that this is feasible and it is planned to increase the frame rate to about 400 Hz. Owing to the success of the method, measurements at other beamlines are planned, and the system will become a standard diagnostic tool for several beamlines.

References

Alkire, R., Rosenbaum, G. & Evans, G. (2000). *J. Synchrotron Rad.* **7**, 61–68.

Bergonzo, P., Brambilla, A., Tromson, D., Marshall, R. D., Jany, C., Foulon, F., Gauthier, C., Solé, V. A., Rogalev, A. & Goulon, J. (1999). *J. Synchrotron Rad.* **6**, 1–5.

Billing, M. G. (1988). *Nucl. Instrum. Methods Phys. Res. A*, **266**, 144–154.

Böge, M. (2004). *Proceedings of the 9th Particle Accelerator Conference, EPAC2004*, 5–7 July 2004, Lucerne, Switzerland, pp. 211–215.

Fajardo, P. & Ferrer, S. (1995). *Rev. Sci. Instrum.* **66**, 1879–1881.

Heald, S. M. (1986). *Nucl. Instrum. Methods Phys. Res. A*, **246**, 411–412.

Holldack, K., Ponwitz, D. & Peatman, W. B. (2001). *Nucl. Instrum. Methods Phys. Res. A*, **467–468**, 213–220.

Karlin, B. A., Cowan, P. L. & Woicik, J. C. (1992). *Rev. Sci. Instrum.* **63**, 526–529.

Koch, A. & Riekel, C. (1996). *Rev. Sci. Instrum.* **67**, 1737–1740.

Kudo, T. P., Aoyagi, H., Sato, K., Wu, S., Tanaka, H., Sasaki, S., Nakatani, T., Takeuchi, M., Shimada, T., Hiramatsu, Y., Yokoya, A., Agui, A., Yoshigoe, A., Ohkuma, H., Miyahara, Y., Ishikawa, T. & Kitamura, H. (2001). *Nucl. Instrum. Methods Phys. Res. A*, **467–468**, 239–243.

Lurio, L. B., Lumma, D., Sandy, A. R., Borthwick, M. A., Falus, P., Mochrie, S. G. J., Pelletier, J. F., Sutton, M., Regan, L., Malik, A. & Stephenson, G. B. (2000). *Phys. Rev. Lett.* **84**, 785–788.

Mortazavi, P., Woodle, M., Rarback, H., Shu, D. & Howells, M. (1986). *Nucl. Instrum. Methods Phys. Res. A*, **246**, 389–393.

Patterson, B. D., Abela, R., Auderset, H., Chen, Q., Fauth, F., Gozzo, F., Ingold, G., Kühne, H., Lange, M., Maden, D., Meister, D., Pattison, P., Schmidt, T., Schmitt, B., Schulze-Briese, C., Shi, M., Stampanoni, M. & Willmott, P. R. (2005). *Nucl. Instrum. Methods Phys. Res. A*, **540**, 42–67.

Pfeiffer, F., Bunk, O., Schulze-Briese, C., Diaz, A., Weitkamp, T., David, C., van der Veen, J. F., Vartanyants, I. & Robinson, I. K. (2005). *Phys. Rev. Lett.* **94**, 164801.

Sakae, H., Aoyagi, H., Oura, M., Kimura, H., Ohata, T., Shiwaku, H., Yamamoto, S., Tanabe, K., Kobashi, K. & Kitamura, H. (1997). *J. Synchrotron Rad.* **4**, 204–209.

Schilcher, T., Böge, M., Keil, B., Pollet, P. & Schlott, V. (2004). *Proceedings of the 9th Particle Accelerator Conference, EPAC2004*, 5–7 July 2004, Lucerne, Switzerland, pp. 2523–2525. Lucerne, Switzerland.

Schildkamp, W. & Pradervand, C. (1995). *Rev. Sci. Instrum.* **66**, 1956–1959.

Schulze-Briese, C., Ketterer, B., Pradervand, C., Brönnimann, C., David, C., Horisberger, R., Puig-Molina, A. & Graafsma, H. (2001). *Nucl. Instrum. Methods Phys. Res. A*, **467–468**, 230–234.

Shu, D., Ding, H., Barraza, J., Kuzay, T. M., Haeffner, D. & Ramanathan, M. (1998). *J. Synchrotron Rad.* **5**, 632–635.

Silfhout, R. G. van (1999). *J. Synchrotron Rad.* **6**, 1071–1075.

Tischler, J. & Hartman, P. L. (1980). *Nucl. Instrum. Methods*, **171**, 67–71.

Xie, Y., Hu, T. D., Liu, T. & Xian, D. C. (2001). *Nucl. Instrum. Methods Phys. Res. A*, **467–468**, 256–259.